

Probing magnetoelastic effects of ultrathin antiferromagnets via magnetic domain imaging in ferromagnetic-antiferromagnetic bilayers

Bo-Yao Wang,^{1,*} Jhen-Yong Hong,² Nae-You Jih,² Kui-Hon Ou Yang,² Li-Ren Chen,² Hong-Ji Lin,³ Yuet-Loy Chan,³ Der-Hsin Wei,³ and Minn-Tsong Lin^{2,4,†}

¹*Department of Physics, National Changhua University of Education, Changhua 500, Taiwan*

²*Department of Physics, National Taiwan University, Taipei 106, Taiwan*

³*National Synchrotron Radiation Research Center, Hsinchu 300, Taiwan*

⁴*Institute of Atomic and Molecular Sciences, Academia Sinica, Taipei 106, Taiwan*

(Received 2 August 2014; published 29 December 2014)

We report an experimental investigation of the magnetoelastic effects of ultrathin antiferromagnets, performed by comparing the characteristic behavior of the induced spin-reorientation transition (SRT) of Co films in two types of epitaxially grown bilayers: face-centered-cubic (fcc)-like Mn/Co (fcc-Mn: $a = 3.75 \text{ \AA}$, $c = 3.76 \text{ \AA}$) and face-centered-tetragonal (fct)-Mn ($a = 3.61 \text{ \AA}$, $c = 3.78 \text{ \AA}$). Magnetic hysteresis loops and magnetic domain images indicate that both fcc-Mn and fct-Mn films can produce a $\langle 110 \rangle$ to $\langle 100 \rangle$ SRT in adjacent Co films when the thickness of the Mn layer is greater than a temperature-dependent critical value. Detailed analysis of the critical thickness of Mn films and the evolution of the Co domain structure upon SRT indicate that the fct-Mn film had a higher antiferromagnetic ordering temperature and stronger lateral Mn-Mn exchange coupling compared with the fcc-Mn film. The enhanced long-range antiferromagnetic ordering emerging concurrently with the in-plane lattice variation of the fcc-like Mn film in Mn/Co bilayers clearly showed the magnetoelastic effect of ultrathin antiferromagnets.

DOI: [10.1103/PhysRevB.90.224424](https://doi.org/10.1103/PhysRevB.90.224424)

PACS number(s): 75.50.Ee, 75.30.Gw, 75.70.Kw, 75.70.Rf

I. INTRODUCTION

Antiferromagnets, a class of magnetic materials with compensated magnetization, are well known for their property of controlling the magnetic properties of adjacent ferromagnetic (FM) thin films through interfacial exchange coupling. In magnetologic devices such as the spin valve, the effects of exchange bias fields and coercivity enhancement are extensively used for “pinning” the magnetization of magnetic reference layers [1–5]. Recent studies have reported that antiferromagnetic (AFM) thin films can alter the magnetization direction of the adjacent FM layer, leading to a spin reorientation transition (SRT) that depends on the characteristics or symmetry of the interfacial moments [6–12]. Such a mechanism can even induce perpendicular magnetization [11–14], thus enhancing the functionality of AFM thin films.

It is known that the magnetic properties of a magnetic material could be sensitive to deformations in the crystalline structure or variations in the lattice parameter because of the modification of the orientation of spin-orbital coupling or the strength of exchange coupling (i.e., magnetoelastic effects). In an FM thin film, such effects are known to cause the so-called magnetoelastic anisotropy, which could alter the direction of the magnetic easy axis, depending on the orientation and degree of lattice strain [5,15–17]. For AFM thin films, direct probing of antiferromagnetism is extremely challenging because of the lack of macroscopic magnetization. Although the antiferromagnetism of AFM films may be inferred from the magnetic response of FM films in AFM-FM bilayers [6–10], the effects on FM films themselves and the possible

morphological (or interface) effects must be appropriately excluded when studying the magnetoelastic effects of AFM films. Our knowledge of magnetoelastic effects of AFM films is limited, probably because of the challenges involved in experimentally probing the correlation between variations in the crystallinity and antiferromagnetism. Although a previous study suggested that the exchange bias field in FM/AFM bilayers could be enhanced by reducing the vertical interlayer distance in the AFM thin film [18], the magnetoelastic effects of an antiferromagnet with in-plane lattice variations, which is generally crucial when the epitaxial growth technique is used for crystal engineering of the magnetic properties of magnetic samples, are still unclear.

Among various antiferromagnets, face-centered-cubic (fcc)-like Mn thin films are considered to be highly attractive systems because they can be fabricated with current epitaxial growth techniques [19–26]. Although theoretical studies have suggested that the behavior of bulk fcc-like Mn could be a function of the lattice parameters, on the basis of the rich magnetic phase diagram of bulk fcc-like Mn [27,28], for Mn thin films directly grown on FM films with stable in-plane magnetization (or vice versa), experiments involving spin-polarized scanning tunneling microscopy (SP-STM) and x-ray magnetic circular dichroism (XMCD)-based photoemission microscopy (PEEM) have supported in-plane layered AFM structures [10,23,24,29]. The similar AFM structure of Mn films in fcc-like Mn/FM bilayers renders them relatively simple model systems that can be used for exploring the magnetoelastic effects of antiferromagnets. Because the phenomenon of antiferromagnetism-induced SRT in AFM/FM bilayers has been reported to be highly sensitive to variations in the magnetic anisotropy or spin ordering of the AFM ultrathin film [6–8,10], this phenomenon can be possibly used to determine the magnetoelastic effects of fcc-like Mn ultrathin antiferromagnets.

*bywang1735@cc.ncue.edu.tw

†mtlin@phys.ntu.edu.tw

In this study, the magnetoelastic effects of fcc-like Mn films are investigated by comparing the characteristic behavior of the Mn-induced $\langle 110 \rangle$ to $\langle 100 \rangle$ SRT in Co films in two types of bilayers: epitaxially grown fcc-Mn/Co and face-centered-tetragonal (fct)-Mn/Co bilayers (fcc-Mn: $a = 3.75 \text{ \AA}$, $c = 3.76 \text{ \AA}$; fct-Mn: $a = 3.61 \text{ \AA}$, $c = 3.78 \text{ \AA}$). We show that there is an appreciable increase in the AFM ordering temperature and enhancement of the lateral Mn-Mn exchange coupling on fcc-like Mn films when the in-plane lattice constant is reduced. This finding provides experimental evidence of magnetoelastic effects of low-dimensional antiferromagnets, whose observation with conventional approaches continues to pose a challenge.

II. EXPERIMENT

Magnetic ultrathin films were prepared in an ultrahigh vacuum NTU-NSRRC nanomagnetism preparation chamber through thermal evaporation at a base pressure of 2×10^{-10} Torr. Single crystals of $\text{Cu}_3\text{Au}(001)$ ($a = 3.75 \text{ \AA}$) and $\text{Cu}(001)$ ($a = 3.61 \text{ \AA}$) with a 0.1° miscut were used as the substrates, and they were prepared using procedures described in previous reports [10,16,17]. Depending on the objectives of different experiments, either uniform or wedge-shaped Mn/Co bilayers were deposited on the substrates at room temperature. The growth rates were monitored by using medium energy electron diffraction, and a layer-by-layer growth mode was observed for five-monolayer (ML) Co films grown on $\text{Cu}_3\text{Au}(001)$ and $\text{Cu}(001)$, and Mn films grown on Co layers, as described in detail in the Supplemental Material [30]. The average in-plane and interlayer distances of the films were determined by using low-energy electron diffraction (LEED) with the kinematics approximation (LEED I/V) [31].

The magnetic domain images of Mn/Co bilayers were obtained *in situ* through PEEM [32,33] by using the XMCD effects at beam line BL05B2 of the National Synchrotron Radiation Research Center (NSRRC) in Hsinchu, Taiwan. The angles of incident right circularly polarized (RCP) x rays with respect to the in-plane $[0\bar{1}0]$ crystallographic direction of $\text{Cu}_3\text{Au}(001)$ and $\text{Cu}(001)$ were 5° and 0° , respectively [34], and 25° relative to the surface plane. As described in a previous study [5], the magnetic information of individual elements can be obtained from the asymmetry of the XMCD curve at the $L_{3,2}$ absorption edges. The full-field view of the secondary electrons emitted from the magnetic sample was resolved by combining XMCD and PEEM and by using a multichannel plate, and the full-field view was recorded using a CCD camera. Contrast normalization was achieved by performing imaging calculations for the two full-field images taken at the Co L_3 and L_2 edges [10]. In the current study, magnetic imaging was performed in the as-grown condition at either 300 or 106 K. The XMCD curves were obtained in beam line BL11A1 of the NSRRC; they were derived from the $L_{3,2}$ -edge x-ray absorption spectra at ± 2600 Oe with a fixed incident x-ray polarization of approximately 78% in the total electron yield (TEY) mode. The element-resolved magnetic hysteresis loops, acquired by recording the magnetic asymmetry at the $L_{3,2}$ absorption edges in the x-ray absorption spectra for different magnetic fields, were also measured in the TEY mode at 80 K. Since previous studies have reported

that the uncompensated magnetic moments of the Mn film in Mn/Co/Cu(001) are present only when the Mn thickness (t_{Mn}) is less than 2 ML [26,35], in the current study, we focused on uncompensated Mn moments in Mn/Co/Cu₃Au(001).

III. RESULTS

A. Crystalline structure of Mn/Co/Cu₃Au(001) and Mn/Co/Cu(001)

In this section, we first present a brief introduction of the crystalline structure of Mn/Co bilayers grown on $\text{Cu}_3\text{Au}(001)$ and $\text{Cu}(001)$. Figures 1(a)–1(d) show the selected LEED patterns of $\text{Cu}_3\text{Au}(001)$, subsequently deposited 5 ML Co films, and Mn films grown on 5 ML Co bilayers. The LEED $P(1 \times 1)$ spots of these films are clearly located at the same positions as that of $\text{Cu}_3\text{Au}(001)$, indicating epitaxial growth conditions. The in-plane lattice constant (d_{\parallel}) of the grown Mn/Co bilayers is equal to the $\text{Cu}_3\text{Au}(001)$ value (approximately 3.75 \AA). Similarly to the aforementioned case, Figs. 1(e)–1(h) indicate that the positions of the $P(1 \times 1)$ LEED spots of $\text{Cu}(001)$ and the grown Mn/Co bilayers are identical, implying epitaxial growth conditions for the Mn/Co films grown on $\text{Cu}(001)$. The parameter d_{\parallel} of the Mn/Co bilayers can therefore be obtained from the $\text{Cu}(001)$ value (approximately 3.61 \AA). We observe a dim structure around the $P(1 \times 1)$ spots of the LEED pattern in 5 ML Co/Cu₃Au(001). This implies the presence of a slight corrugation on the surface of the Co film [36,37], and this may be attributed to a relatively higher lattice mismatch between Co and $\text{Cu}_3\text{Au}(001)$ (-5.6%) [17] compared with Co and $\text{Cu}(001)$ (-1.9%) [38–40].

Figures 2(a) and 2(b) show the LEED specular spot I/V curves and interlayer distance for Mn films grown on 5 ML Co/Cu₃Au(001) and 5 ML Co/Cu(001), respectively. The Mn films show invariant d_{\perp} of 1.88 ± 0.015 and $1.89 \pm 0.015 \text{ \AA}$, respectively. Figure 2 shows the overall crystalline structure of both types of Mn films, obtained by combining the results of d_{\parallel} . Clearly, d_{\perp} of these Mn films are quite close. A slightly increase in d_{\perp} for the Mn films grown on Co/Cu(001) may result from the elastic effect of the Mn crystal because of its considerably shortened in-plane atomic distance. The crystalline structure of the Mn films can be conventionally classified on the basis of the ratio of the vertical and in-plane lattice constants (i.e., the c/a ratio). In the present case, the c/a ratios close to 1.00 and 1.05 indicate the fcc and fct structures of the Mn films grown on Co/Cu₃Au(001) and Co/Cu(001). The c/a ratios of the 5 ML Co films grown on $\text{Cu}_3\text{Au}(001)$ and $\text{Cu}(001)$ were approximately 0.89 and 0.97, respectively, and these films were classified as having fct structures.

B. Magnetic properties and induced [100] magnetic anisotropy in fcc-like Mn/Co bilayers

In this section, the magnetic properties of fcc-like Mn/Co bilayers grown on either $\text{Cu}_3\text{Au}(001)$ or $\text{Cu}(001)$ substrates are first introduced. Figures 3(a) and 3(b) show the magnetic hysteresis loops of 5 ML Co/Cu₃Au(001) and 5 ML Co/Cu(001), respectively, measured along the in-plane $[110]$ and $[100]$ directions. In both Co films, when the hysteresis loops were measured along the $[110]$ direction, the remanent magnetization was nearly equal to the saturation

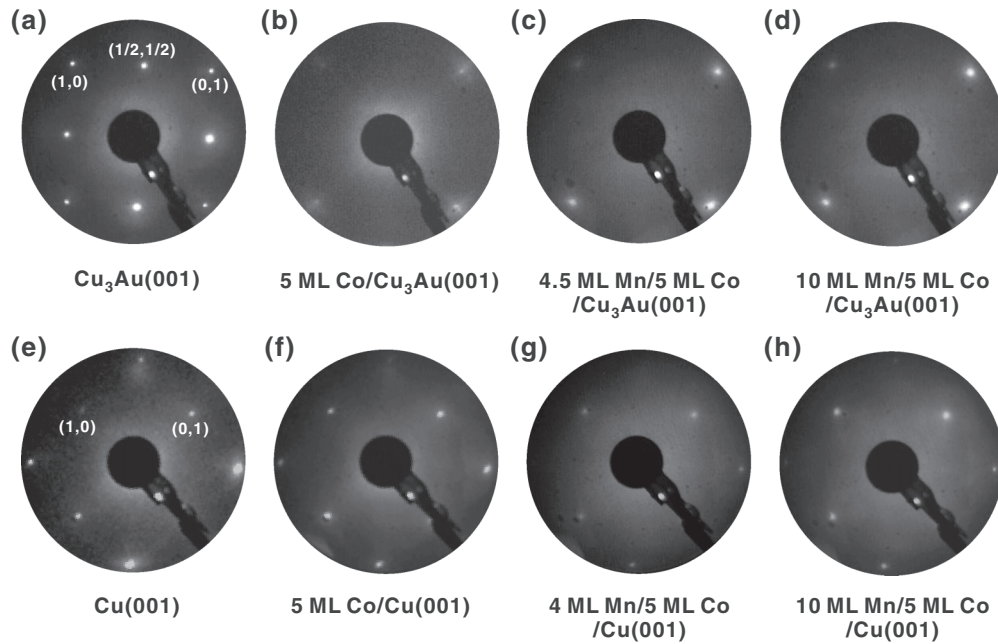


FIG. 1. LEED patterns of (a) Cu₃Au(001), (b) 5 ML Co/Cu₃Au(001), (c) 4.5 ML Mn/5 ML Co/Cu₃Au(001), and (d) 10 ML Mn/5 ML Co/Cu₃Au(001) obtained at 60 eV, and LEED patterns of (e) Cu(001), (f) 5 ML Co/Cu(001), (g) 4 ML Mn/5 ML Co/Cu(001), and (h) 10 ML Mn/5 ML Co/Cu(001) measured at 110 eV.

magnetization; however, the remanent magnetization was lower when the hysteresis loops were measured along the [100] direction. This indicates that the magnetic easy axis for the fct-like Co films is [110], which is consistent with the results obtained in previous studies [7,8].

Figure 3(c) clearly shows that both 4.5 ML Mn/Co bilayers had enhanced H_c compared with the Co films alone. In an exchange-coupled AFM/FM bilayer with established AFM ordering, it is commonly accepted that the AFM layer can induce additional magnetic anisotropy in an adjacent FM

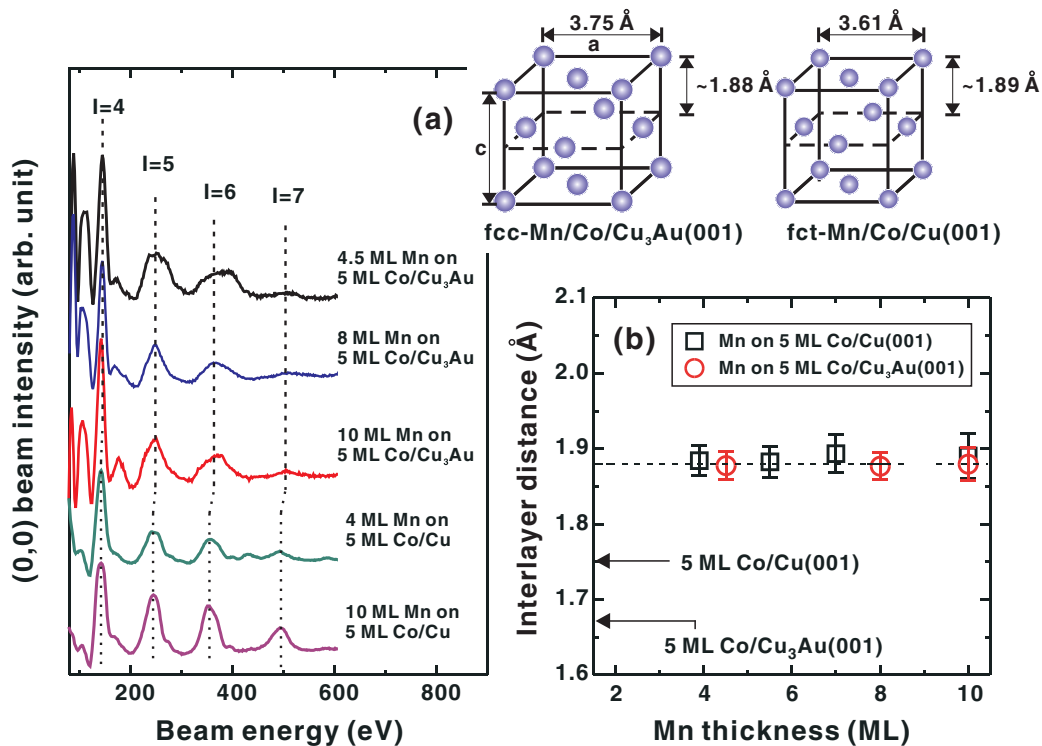


FIG. 2. (Color online) (a) Selected LEED specular spot I/V curves for various Mn films grown on 5 ML Co/Cu₃Au(001) and 5 ML Co/Cu(001). (b) The average interlayer distance (d_{\perp}) of various films calculated according to the energy peaks (I) in the I/V curves. In (b), the arrows represent d_{\perp} of 5 ML Co films grown on Cu₃Au(001) and Cu(001). At the top, the crystalline structures of the fcc-Mn and fct-Mn films, determined from the LEED and LEED I/V analysis, are shown.

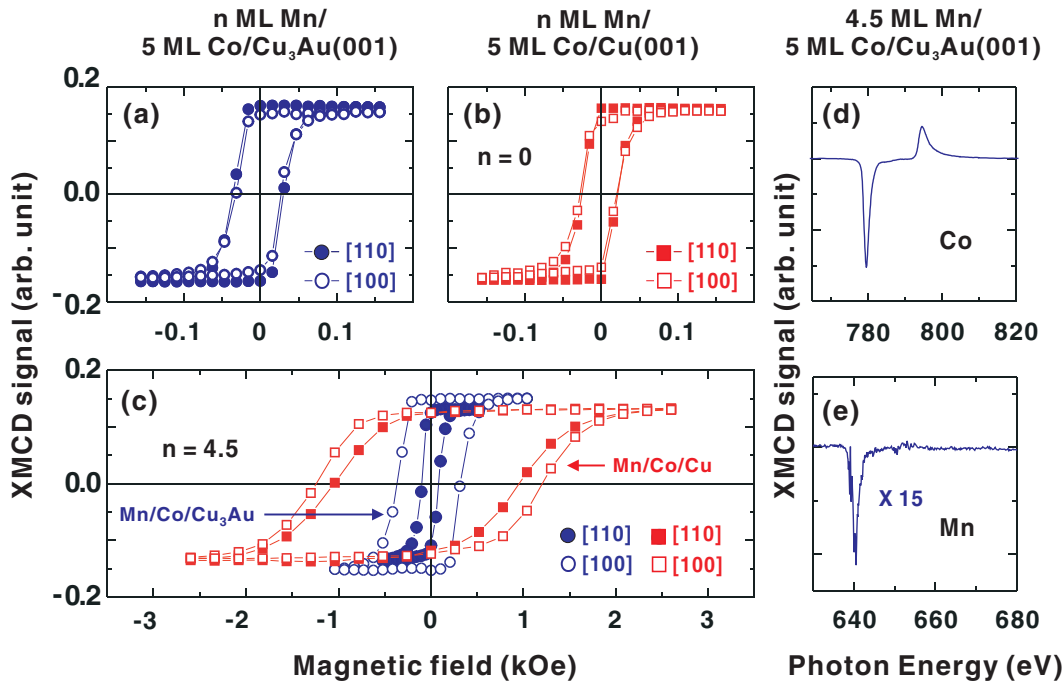


FIG. 3. (Color online) Magnetic hysteresis loops of (a) 5 ML Co/Cu₃Au(001), (b) 5 ML Co/Cu(001), and (c) 4.5 ML Mn/5 ML Co/Cu₃Au(001) (blue), and 4.5 ML Mn/5 ML Co/Cu(001) (red) measured along the [110] and [100] directions, at 80 K [49]. (d), (e) $L_{3,2}$ -edge XMCD curves of Co and Mn for 4.5 ML Mn/5 ML Co/Cu₃Au(001), respectively, for 80 K. The element-specific hysteresis loops were measured in the TEY mode by recording the x-ray absorption intensity at the $L_{3,2}$ edges with the normalization formula $(L_3 - L_2)/(L_3 + L_2)$.

film [9,41–43]. Moreover, the coercivity of the FM film could be significantly enhanced because of increase of domain-wall activated processes caused by the pinning effects from the AFM layer [1,5]. Thus, the observation of enhanced coercivity in both 4.5 ML Mn/Co bilayers implies that Mn-Co exchange coupling and long-range AFM ordering of Mn films were present in both systems. Remarkably, H_c of the fct-Mn/Co bilayer was considerably higher than that of the fcc-Mn/Co film. To determine the origin of different coercivity enhancements between the two cases, the effects of interface roughness must be considered first; this is because interface roughness could lead to decreased coercivity in a Mn/Co bilayer [44,45]. In an extreme case, a change in the Mn-Co interface from a perfectly smooth interface (Mn grown on a Co film with an integer number of layers) to a rough interface (Mn film grown on a Co film with a half-integer number of layers) could result in a coercivity decrease of approximately 50% [44,45]. In the present study, a small corrugation may occur on the surface of the 5 ML Co/Cu₃Au(001) because of a relatively high lattice mismatch between Co and Cu₃Au(001) (-5.6%). This could result in a slightly rougher interface in Mn/Co/Cu₃Au(001) compared with the interface of Mn/Co/Cu(001). However, as illustrated in Fig. 3(c), the coercivity of 4.5 ML Mn/5 ML Co/Cu₃Au(001) is approximately 10% ~ 30% of that of 4.5 ML Mn/5 ML Co/Cu(001). Such a large variation in the coercivity cannot be simply explained by the presence of slight interface roughness in 4.5 ML Mn/5 ML Co/Cu₃Au(001). The different strengths of magnetic coupling between the two Mn films, which result in different magnitudes of Mn-Co exchange coupling in the fct-Mn/Co and fcc-Mn/Co bilayers, should play a crucial role.

Figure 3(c) also clearly indicates that the remanent magnetization and H_c measured along the [100] direction are relatively higher than those measured along the [110] direction. This indicates enhanced [100] magnetic anisotropy for the fcc-like Mn/Co bilayers, which could be caused by the fcc-like Mn films through the Mn-Co exchange coupling. Figures 3(d) and 3(e) illustrate the Co and Mn XMCD curves of 4.5 ML Mn/Co/Cu₃Au(001), respectively, indicating that the Mn film shows uncompensated Mn moments that are coupled in parallel to the Co magnetization. This finding is consistent with the result of the Fe/fcc-Mn/Cu₃Au(001) bilayer [10], and it is in sharp contrast to the absence of uncompensated magnetic moments in Mn/Co/Cu(001) with $t_{\text{Mn}} > 2$ ML [26,35]. This finding therefore provides a crucial clue to the different AFM characteristics between fcc-Mn and fct-Mn films in Mn/Co bilayers, caused by magnetoelastic effects, and is discussed in the Discussion section.

C. Direct observation of SRT via magnetic domain imaging

Detailed information about the magnetic anisotropy of the Co films in fcc-like Mn/Co bilayers can be obtained by performing XMCD-PEEM measurements through direct magnetic domain imaging [32,33]. Because the magnetic anisotropy of Co films could be highly sensitive to a variation in the thickness of the Mn layer, an investigation was conducted on wedge-shaped Mn/Co bilayers (Fig. 4, top illustrations). Figures 4(a) and 4(b) illustrate the Co-domain images of the wedge-shaped fcc-Mn/Co and fct-Mn/Co bilayers, respectively, measured at 300 K. By averaging the regions bounded by dashed lines of Figs. 4(a)–4(d), the magnetic asymmetry

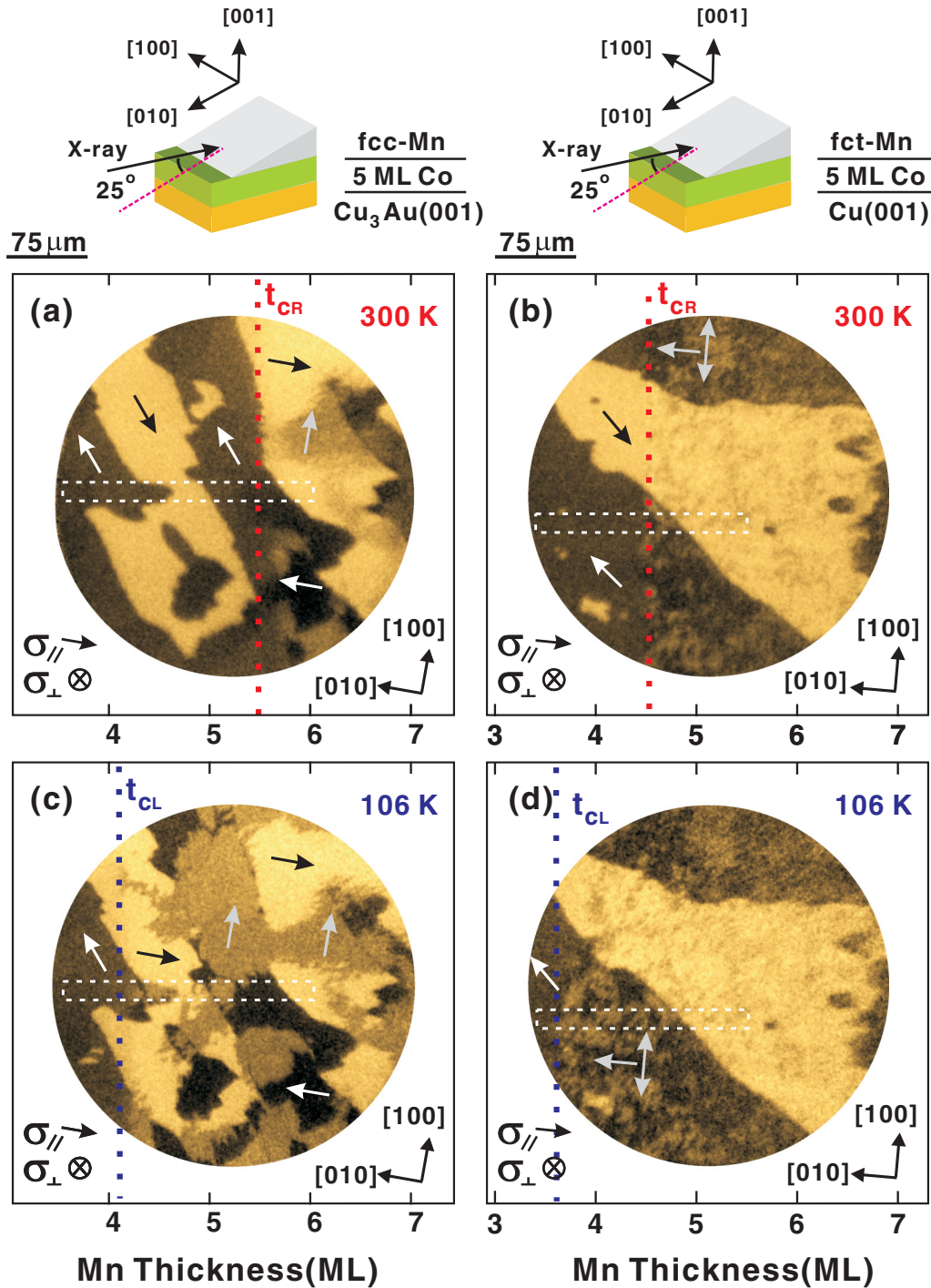


FIG. 4. (Color online) Co domain images of (a) wedge-shaped Mn/5 ML Co/Cu₃Au(001) and (b) wedge-shaped Mn/5 ML Co/Cu(001) obtained with RCP x-rays at 300 K. (c), (d) Magnetic domain images of wedge-shaped Mn/5 ML Co/Cu₃Au(001) and wedge-shaped Mn/5 ML Co/Cu(001) measured at 106 K, respectively. The arrows indicate the magnetization orientation of the magnetic domains, estimated from the normalized XMCD asymmetry profiles (I_A) derived from the region bounded by white dashed lines [Figs. 5(a) and 5(b)]. In (b) and (d), the magnetic direction of the individual $\langle 100 \rangle$ magnetic domain is not indicated by arrows because of a frustrated structure. In both systems, the magnetization orientation is changed from $\langle 110 \rangle$ to $\langle 100 \rangle$ when t_{Mn} is greater than the thickness thresholds (indicated by t_{CL} or t_{CR}).

as a function of t_{Mn} at different temperatures can be obtained. In the XMCD theory, the magnetic asymmetry is proportional to the inner product of the photohelicity vector $\vec{\sigma}$ and the magnetic moment density \vec{M} , according to $I_A = \vec{\sigma} \cdot \vec{M} = \sigma_{||} M \cos \theta$ [5,10]. In the present work, the magnetic asymmetry

is normalized by $\sigma_{||}$ and M with assumption of constant values. Therefore, the value of derived normalized magnetic asymmetry (I_A) can be applied to obtain the magnetization direction of the Co films as a function of t_{Mn} , as shown in the illustrations of Figs. 5(a) and 5(b).

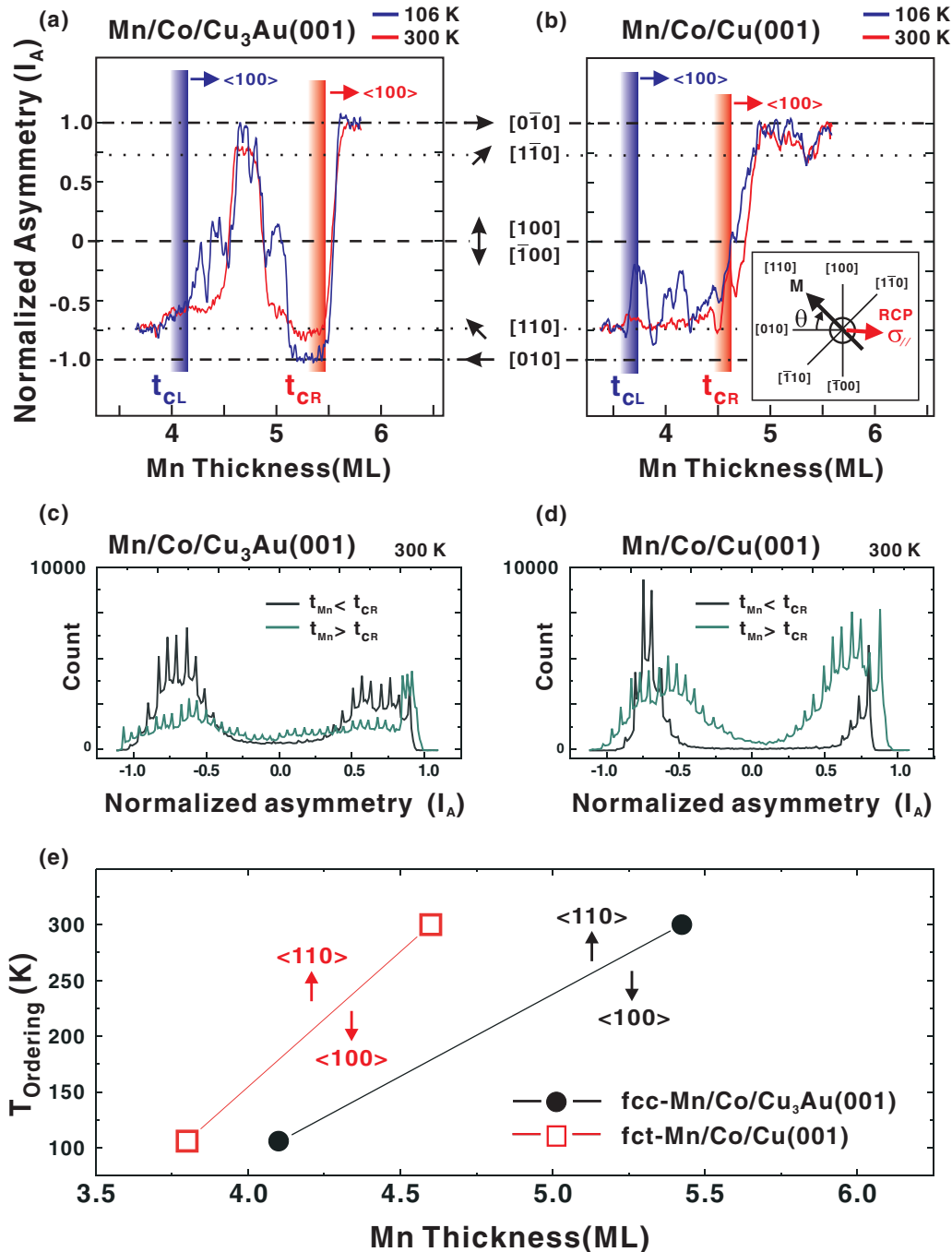


FIG. 5. (Color online) (a), (b) The I_A curves of the wedge-shaped Mn/5 ML Co/Cu₃Au(001) and wedge-shaped Mn/5 ML Co/Cu(001), respectively, extracted from Figs. 4(a)–4(d). In both systems, the thickness thresholds of the SRT decreased from t_{CR} to t_{CL} when the temperature decreased from 300 K to 106 K. (c), (d) The histogram analysis of Figs. 4(a) and 4(b) at the regions of the t_{Mn} below and above the t_{CR} . (e) The magnetic ordering temperature ($T_{ordering}$) as a function of t_{Mn} for both fcc-Mn/Co and fct-Mn/Co bilayers, deduced from the phenomenon of induced SRT.

For the wedge-shaped fcc-Mn/Co bilayer at 300 K [Fig. 4(a)], two characteristic Co magnetization directions (i.e., [110] and $[\bar{1}\bar{1}0]$) were clearly present as t_{Mn} at a low coverage. When t_{Mn} is greater than a threshold value of approximately 5.4 ML (indicated by t_{CR}), the magnetization direction of the magnetic domain changes from $\langle 110 \rangle$ to $\langle 100 \rangle$, reflecting an SRT of the Co film in the fcc-Mn/Co bilayer. Furthermore, the wedge-shaped fct-Mn/Co bilayer demonstrates a similar SRT behavior [Fig. 4(b)], but with a lower Mn-film threshold

(approximately 4.6 ML) and a considerably reduced Co domain size. Such a result can further be confirmed from a histogram analysis of the I_A level at the regions of the t_{Mn} below and above the t_{CR} , as displayed in Figs. 5(c) and 5(d). As the t_{Mn} is below the t_{CR} , it is clear that the I_A of both systems is distributed approximately at ± 0.7 , corresponding to the $\langle 110 \rangle$ magnetization [46]. The distribution of the I_A is much broader and extends to 0 and ± 1 as the t_{Mn} is above the t_{CR} , probably because of the presence of $\langle 100 \rangle$ -oriented

magnetic domains. These results clearly indicate the general features of induced $\langle 100 \rangle$ magnetic anisotropy on Co films covered with fcc-like Mn films, which are consistent with our hysteresis loop measurements (Fig. 3).

As shown in Fig. 4, the SRT in Co films is triggered when t_{Mn} is higher than a threshold value (t_{CR} or t_{CL}). Moreover, we observed that the threshold value decreased from t_{CR} to t_{CL} when the temperature changed from 300 K to 106 K, respectively. Such a forward threshold shift with a decrease in the temperature is attributed to the presence of long-range AFM ordering in the Mn layer in the t_{CR} to t_{CL} region at 106 K, which could be a paramagnetic state at 300 K [10,47]. It is noted that the onset t_{Mn} of AFM ordering of the presented fct-Mn/Co/Cu(001) film at 300 K is higher than that observed in previous studies (approximately 2 ML) [19,26]. The reason for this difference could be attributed to a slightly different surface morphology or crystalline structure of the Mn film, caused by the different preparation temperatures or different miscut angles of the Cu(001) substrate. Thus, our results provide crucial evidence that the $\langle 110 \rangle$ to $\langle 100 \rangle$ SRT in the Co film in fcc-like Mn/Co bilayers is induced by the antiferromagnetism of fcc-like Mn layers, modulated by finite-size effects [47]. With this relationship, the degree of long-range AFM ordering for a specific thickness of the fcc-like Mn film in Mn/Co bilayers can be probed by measuring the critical temperature that induces SRT. In Figs. 4 and 5, because t_{CR} and t_{CL} are the thickness thresholds for the presence of AFM ordering in the Mn layer at 300 K and 106 K, respectively, the magnetic ordering temperature (T_{ordering}) of fcc-like Mn films with thicknesses t_{CR} and t_{CL} can be inversely estimated. As summarized in Fig. 5(e), the fct-Mn film shows a higher T_{ordering} compared with the fcc-Mn film in the displayed t_{Mn} range. This finding is highly consistent with the results of our hysteresis-loop measurements (Fig. 3), which indicates that the fct-Mn film can show a higher degree of H_c enhancement and Mn-Co exchange coupling than the fcc-Mn film in fcc-like Mn/Co bilayers.

IV. DISCUSSION

A. Long-range AFM ordering probed by magnetic domain imaging

The long-range AFM ordering of two types of fcc-like Mn films can be further probed by examining the domain-structure variation in adjacent Co films as the Mn-induced $\langle 110 \rangle$ to $\langle 100 \rangle$ SRT occurs. In the ideal case of an AFM/FM coupled bilayer with a perfectly flat interface and a layered AFM spin structure, the magnetization of the FM film is coupled to be collinear with the alternatively aligned layered spins of the AFM layer at the interface. The domain structure of the FM film in this type of AFM/FM bilayer is mainly determined by minimizing the stray field energy of the FM film, and the FM film size could reach tens or hundreds of micrometers, similar to an individual FM film [5]. However, in practical AFM/FM systems, the roughness of the interface inherent from the terrace or grain boundary of the substrate could lead to a perturbation in the long-range magnetic ordering of the AFM/FM bilayer. Induced magnetic frustration could appear in either the AFM or the FM layer, depending on the relative

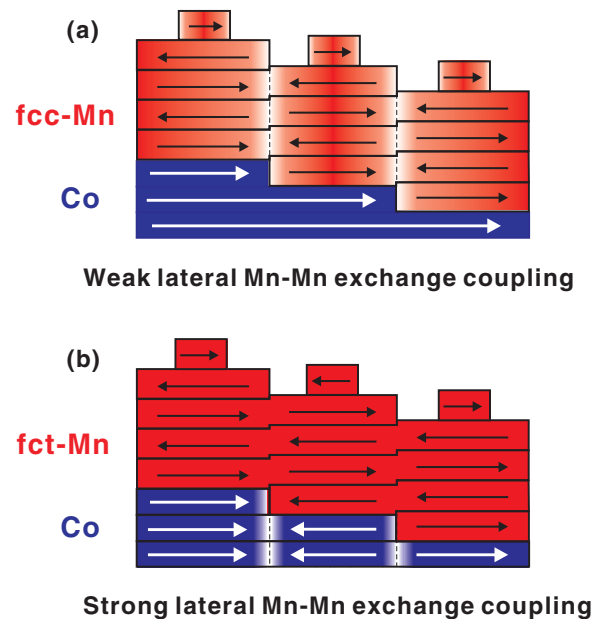


FIG. 6. (Color online) Two schematic models of Mn/Co exchange-coupled bilayer systems with (a) Mn-Mn exchange coupling \ll Co-Co exchange coupling and (b) Mn-Mn exchange coupling \gg Co-Co exchange coupling. A single atomic step is used in both models for simulating the presence of interface roughness inherent in the grain boundary or substrate terrace. In (b), the magnetic direction of the uncompensated Mn moments on different Co steps could be oppositely directed and could compensate each other, because of strong lateral Mn-Mn exchange coupling.

strength of the lateral exchange coupling for the two layers [5,7,8,24].

For a case in which the lateral exchange coupling of the AFM layer is considerably weaker than that of the FM layer [Fig. 6(a)], the magnetic frustration induced by the substrate terrace could occur in the AFM layer. The shape and size of the FM domain in such an AFM/FM bilayer could be less perturbed and similar to the case of the individual FM film. Furthermore, if the lateral exchange coupling of the AFM layer is considerably stronger than that of the FM layer [Fig. 6(b)], the presence of robust long-range spin ordering in the AFM film could lead to the formation of a twin-phase spin arrangement of the Mn film at the AFM-FM interface. This could substantially reduce the domain size of the adjacent FM layer because of the established collinear coupling and biquadratic coupling. Because the experimental results obtained in previous studies have indicated a layered-AFM structure of Mn films in fcc-like Mn/FM bilayers [10,29], in the current study, the strength of the long-range lateral exchange coupling between fcc-Mn and fct-Mn films can be distinguished by monitoring the features of the AFM-induced domain evolution.

In the case of the wedge-shaped fcc-Mn/Co bilayer [Figs. 4(a) and 4(c)], the size and general shape of the induced $\langle 100 \rangle$ magnetic domains are nearly identical to the preceding $\langle 110 \rangle$ domains, with a typical domain size larger than $50 \mu\text{m}$. This indicates that the lateral Mn-Mn exchange coupling is relatively weaker than the lateral Co-Co exchange coupling. By contrast, for the case of a wedge-shaped fct-Mn/Co bilayer

[Figs. 4(b) and 4(d)], the size of the induced $\langle 100 \rangle$ magnetic domains was considerably smaller than that of the preceding $\langle 110 \rangle$, suggesting that the strength of the lateral exchange coupling in the Mn layer could be considerably stronger than that in the Co film.

To further compare the magnitude of Mn-Mn exchange coupling between fcc-Mn/Co and fct-Mn/Co films, the Co-Co exchange coupling and the Mn-Co exchange coupling between two systems need to be characterized first. According to theoretical calculation on tetragonal Co [48], the Co magnetic moments evolve slowly upon variations of the c/a ratio and crystalline volume in the fct regime. This suggests that a slight crystalline distortion in fct-Co film cannot result in a significant modulation on magnetic moment of Co as well as the Co-Co exchange coupling. In the present case, since the variation of crystalline volume of fct-Co film grown on $\text{Cu}_3\text{Au}(001)$ and $\text{Cu}(001)$ films is only 2.8%, we can assume that the Co-Co exchange coupling remains constant between two systems. On the other hand, the strength of Mn-Co exchange coupling could be associated with two factors: (1) Mn-Co interface condition, and (2) Mn-Mn exchange coupling from the entire Mn film according to the finite-size effects [47]. Since the former factor has been concluded to be nonsignificant in the present work, we can assume that its effect on Co-Mn exchange coupling stays unchanged between two systems. The strength of Mn-Co exchange coupling is therefore dominated by the latter factor.

Thus, by considering the deviation of the domain size of Co in the Mn/Co bilayer and by assuming that the difference in exchange coupling between two types of Co films is negligible, we can deduce that the lateral exchange coupling in the fct-Mn film was considerably stronger than that in the fcc-Mn film. This finding also indicates the cause of the higher AFM ordering temperature in the fct-Mn film compared with the fcc-Mn film in the Mn/Co bilayer [Fig. 5(c)].

B. Correlation of AFM structure and uncompensated Mn moments in fcc-like Mn/Co bilayers

As mentioned in the previous section, the results obtained in the current study support an in-plane layered AFM structure for the fcc-like Mn thin films grown on in-plane magnetic FM films (or vice versa) [10,23,24,29]. In the case of the fcc-Mn thin film, a previous XMCD-PEEM study on in-plane magnetic Fe/fcc-Mn/ $\text{Cu}_3\text{Au}(001)$ reported the presence of uncompensated magnetic moments in the Mn layer [10]; this study also observed the presence of an uncompensated-compensated transition of the Mn magnetic interface along with the continuous variation of t_{Mn} . This provides evidence of a layered AFM structure for the Mn film in the Fe/fcc-Mn bilayer. In the current study involving fcc-Mn/Co/ $\text{Cu}_3\text{Au}(001)$, uncompensated Mn moments coupled in parallel to the Co magnetization were observed [Figs. 3(d) and 3(e)]. This result is consistent with the finding for the Fe/fcc-Mn bilayer, thus supporting a layered AFM structure for the fcc-Mn film grown on Co/ $\text{Cu}_3\text{Au}(001)$. For the case of Mn/Co/ $\text{Cu}(001)$, previous reports have suggested that the uncompensated magnetic moments of the Mn film cannot be observed when t_{Mn} is greater than 2 ML [26,35]. Although there is no XMCD signal observed for a thicker fct-Mn/Co/ $\text{Cu}(001)$, the results of a microscopic investigation using SP-STM indicated a clearly

layered spin contrast for 3.5 ML Mn/Co/ $\text{Cu}(001)$ at 77 K [29]. This finding provides direct evidence of the fct-Mn film grown on Co/ $\text{Cu}(001)$ having a layered AFM structure.

According to the preceding discussion, there is a discrepancy between the XMCD and SP-STM results with regard to the fct-Mn/Co/ $\text{Cu}(001)$ measurements because the Mn film with a layered AFM structure must show uncompensated magnetic moments, which can be detected by the XMCD. In fact, past study of using SP-STM has observed spin frustration across the same Mn layer induced by a hidden Co step [29]. This could cause the cancellation of uncompensated moments of the Mn film grown on different Co steps [Fig. 6(b); schematic diagram], thus explaining the absence of the XMCD signal for the thicker fct-Mn/Co/ $\text{Cu}(001)$. The preceding discussion raises another crucial question: why does the XMCD signal vanish in fct-Mn/Co/ $\text{Cu}(001)$ but continue to be present in fcc-Mn/Co/ $\text{Cu}_3\text{Au}(001)$ [Fig. 3(e)]? This phenomenon can be explained by the main finding of the current study: the lateral exchange coupling of the fcc-Mn film is considerably weaker than that of the fct-Mn film. For the Mn film with a weaker lateral exchange coupling [Fig. 6(a)], the ordering of the layered AFM structure could mainly follow the magnetization direction of the Co step underneath; however, it is less influenced by the Mn films grown on another Co step. Because the uncompensated Mn moments on different Co steps no longer cancel each other, these moments were observed by XMCD.

C. Magnetoelastic effects on fcc-like Mn ultrathin films

As previously highlighted, magnetoelastic effects of a magnetic material can generally cause the strength of long-range magnetic ordering to change, or the magnetoelastic anisotropy to vary. The change in the strength of long-range magnetic ordering is determined by the magnitude of exchange integral sensitive to the distance among the magnetic atoms with localized spins, whereas the variation in the magnetoelastic anisotropy can be correlated with the symmetry of the crystalline structure and the degree of lattice strain [5]. To determine the magnetoelastic effects of the AFM film in AFM/FM bilayers, the effects of FM films themselves and the possible morphological (or interface) effects must be appropriately excluded. Moreover, the possibility of forming different AFM configurations in the Mn films must be considered. In the current study, we provided experimental evidence supporting a layered AFM configuration for Mn films in both fcc-Mn/Co and fct-Mn/Co bilayers [10,29]. We also concluded that the interface and magnetoelastic effects of Co films cannot explain the large reduction in the coercivity of Mn/Co/ $\text{Cu}_3\text{Au}(001)$ compared with Mn/Co/ $\text{Cu}(001)$ [44,45]. Thus, the observed substantial increase in the AFM ordering temperature and the enhanced strength of the lateral Mn-Mn exchange coupling for the fct-Mn film compared with the fcc-Mn film in the Mn/Co bilayers can be attributed to a considerably reduced in-plane atomic distance in the fct-Mn film because of magnetoelastic effects. Previous theoretical studies have proposed that the formation and strength of local magnetic moments in the fcc-like Mn are highly sensitive to the exchange-parameter value and lattice constant [50,51]. The current study confirmed the results of these studies

and provided experimental evidence of the magnetoelastic effects of ultrathin antiferromagnets in more realistic systems. Moreover, from our experimental results, the strong lateral Mn-Mn exchange coupling in the fct-Mn film can explain the long-standing discrepancy between the XMCD [26,35] and SP-STM [29] results regarding the measurement of the AFM state of the Mn film in fct-Mn/Co/Cu(001). Although the current study showed the magnetoelastic effects of ultrathin antiferromagnets only for in-plane magnetic Mn/Co bilayers, future studies should investigate the magnetoelastic effects of Mn/FM bilayers with perpendicular magnetic coupling to understand their influence on perpendicular magnetic anisotropy, which is crucial for developing magnetic devices.

V. CONCLUSION

The present study systemically investigated the magnetoelastic effects of fcc-like Mn ultrathin antiferromagnets

by probing an induced $\langle 110 \rangle$ to $\langle 100 \rangle$ SRT in the Co film in Mn/Co bilayers. A substantially increased AFM ordering temperature and enhanced lateral Mn-Mn exchange coupling were observed when the AFM fcc-like Mn ultrathin films were subjected to in-plane lattice contraction. The results obtained improve our understanding of fundamental antiferromagnetism, which is difficult to probe directly through conventional approaches. The results are also expected to be helpful for the development of next-generation magnetic devices that involve the application of crystal engineering to ultrathin antiferromagnets.

ACKNOWLEDGMENTS

This work was partly supported by the Ministry of Science and Technology, Taiwan (Grants No. NSC 102-2112-M-018-006-MY3 and NSC 100-2120-M-002-002).

-
- [1] J. Nogués and I. K. Schuller, *J. Magn. Magn. Mater.* **192**, 203 (1999).
- [2] S. D. Bader, *Rev. Mod. Phys.* **78**, 1 (2006).
- [3] S. Mao, Z. Gao, H. Xi, P. Kolbo, M. Plumer, L. Wang, A. Goyal, I. Jin, J. Chen, C. Hou, R. M. White, and E. Murdock, *IEEE Trans. Magn.* **38**, 26 (2002).
- [4] W. Zhang, Y. Chen, and C. Hiner, *J. Appl. Phys.* **97**, 10N702 (2005).
- [5] J. Stöhr and H. C. Siegmann, *Magnetism: From Fundamentals to Nanoscale Dynamics* (Springer, New York, 2006), illustrated ed.
- [6] H. Ohldag, A. Scholl, F. Nolting, S. Anders, F. U. Hillebrecht, and J. Stöhr, *Phys. Rev. Lett.* **86**, 2878 (2001).
- [7] W. Kuch, F. Offi, L. I. Chelaru, M. Kotsugi, K. Fukumoto, and J. Kirschner, *Phys. Rev. B* **65**, 140408 (2002).
- [8] C. Won, Y. Z. Wu, H. W. Zhao, A. Scholl, A. Doran, W. Kim, T. L. Owens, X. F. Jin, and Z. Q. Qiu, *Phys. Rev. B* **71**, 024406 (2005).
- [9] Q. F. Zhan and K. M. Krishnan, *Appl. Phys. Lett.* **96**, 112506 (2010).
- [10] B. Y. Wang, C. H. Chuang, S. S. Wong, J. J. Chiou, W. C. Lin, Y. L. Chan, D. H. Wei, and M. T. Lin, *Phys. Rev. B* **85**, 094412 (2012).
- [11] B. Y. Wang, N. Y. Jih, W. C. Lin, C. H. Chuang, P. J. Hsu, C. W. Peng, Y. C. Yeh, Y. L. Chan, D. H. Wei, W. C. Chiang, and M. T. Lin, *Phys. Rev. B* **83**, 104417 (2011).
- [12] B.-Y. Wang, J.-Y. Hong, K.-H. O. Yang, Y.-L. Chan, D.-H. Wei, H.-J. Lin, and M.-T. Lin, *Phys. Rev. Lett.* **110**, 117203 (2013).
- [13] N. Y. Jih, B. Y. Wang, Y. L. Chan, D. H. Wei, and M. T. Lin, *Appl. Phys. Express* **5**, 063008 (2012).
- [14] B. Y. Wang, C. C. Chiu, W. C. Lin, and M. T. Lin, *Appl. Phys. Lett.* **103**, 042407 (2013).
- [15] A. Winkelmann, M. Przybylski, F. Luo, Y. Shi, and J. Barthel, *Phys. Rev. Lett.* **96**, 257205 (2006).
- [16] M. T. Lin, W. C. Lin, C. C. Kuo, and C. L. Chiu, *Phys. Rev. B* **62**, 14268 (2000).
- [17] W. C. Lin, B. Y. Wang, Y. W. Liao, K. J. Song, and M. T. Lin, *Phys. Rev. B* **71**, 184413 (2005).
- [18] W. C. Lin, B. Y. Wang, T. Y. Chen, L. C. Lin, Y. W. Liao, W. Pan, N. Y. Jih, K. J. Song, and M. T. Lin, *Appl. Phys. Lett.* **90**, 052502 (2007).
- [19] J. T. Kohlhepp and W. J. M. de Jonge, *Phys. Rev. Lett.* **96**, 237201 (2006).
- [20] J. T. Kohlhepp, H. Wieldraaijer, and W. J. M. de Jonge, *Appl. Phys. Lett.* **89**, 032507 (2006).
- [21] B. Schirmer, B. Feldmann, A. Sokoll, Y. Gauthier, and M. Wuttig, *Phys. Rev. B* **60**, 5895 (1999).
- [22] C. S. Tian, Z. Tian, J. Wu, G. S. Dong, X. F. Jin, Y. Z. Wu, and Z. Q. Qiu, *J. Magn. Magn. Mater.* **286**, 497 (2005).
- [23] T. K. Yamada, M. M. J. Bischoff, G. M. M. Heijnen, T. Mizoguchi, and H. van Kempen, *Phys. Rev. Lett.* **90**, 056803 (2003).
- [24] U. Schlickum, N. Janke-Gilman, W. Wulfhekel, and J. Kirschner, *Phys. Rev. Lett.* **92**, 107203 (2004).
- [25] W. C. Lin, T. Y. Chen, L. C. Lin, B. Y. Wang, Y. W. Liao, K. J. Song, and M. T. Lin, *Phys. Rev. B* **75**, 054419 (2007).
- [26] M. Caminale, R. Moroni, P. Torelli, W. C. Lin, M. Canepa, L. Mattera, and F. Bisio, *Phys. Rev. Lett.* **112**, 037201 (2014).
- [27] J. Hafner and D. Spišák, *Phys. Rev. B* **72**, 144420 (2005).
- [28] Martin Zelený, F. D. Natterer, A. Biedermann, and J. Hafner, *Phys. Rev. B* **82**, 165422 (2010).
- [29] P.-J. Hsu, C.-I. Lu, Y.-H. Chu, B.-Y. Wang, C.-B. Wu, L.-J. Chen, S.-S. Wong, and M.-T. Lin, *Phys. Rev. B* **85**, 174434 (2012).
- [30] See Supplemental Material at <http://link.aps.org/supplemental/10.1103/PhysRevB.90.224424> for information of the MEED oscillations of the Mn and Co films.
- [31] W. C. Lin, C. C. Kuo, C. L. Chiu, and M.-T. Lin, *Surf. Sci.* **478**, 9 (2001).
- [32] J. Stöhr, Y. Wu, B. D. Hermsmeier, M. G. Samant, G. R. Harp, S. Koranda, D. Dunham, and B. P. Tonner, *Science* **259**, 658 (1993).
- [33] C. M. Schneider and G. Schönhense, *Rep. Prog. Phys.* **65**, 1785 (2002).

- [34] This is caused by a slight difference of sample mounting.
- [35] W. L. O'Brien and B. P. Tonner, *Phys. Rev. B* **50**, 2963 (1994).
- [36] B. Feldmann, B. Schirmer, A. Sokoll, and M. Wuttig, *Phys. Rev. B* **57**, 1014 (1998).
- [37] F. Bisio, S. Terreni, G. Gonella, L. Floreano, A. Morgante, M. Canepa, and L. Mattera, *Phys. Rev. Lett.* **93**, 106103 (2004).
- [38] M. Kowalewski, C. M. Schneider, and B. Heinrich, *Phys. Rev. B* **47**, 8748 (1993).
- [39] Brad N. Engel, C. D. England, R. A. Van Leeuwen, M. H. Wiedmann, and C. M. Falco, *J. Appl. Phys.* **70**, 5873 (1991).
- [40] B. N. Engel, C. D. England, R. A. Van Leeuwen, M. H. Wiedmann, and C. M. Falco, *Phys. Rev. Lett.* **67**, 1910 (1991).
- [41] J. Li, Y. Meng, J. S. Park, C. A. Jenkins, E. Arenholz, A. Scholl, A. Tan, H. Son, H. W. Zhao, C. Hwang, Y. Z. Wu, and Z. Q. Qiu, *Phys. Rev. B* **84**, 094447 (2011).
- [42] Q. F. Zhan, W. Zhang, and K. M. Krishnan, *Phys. Rev. B* **83**, 094404 (2011).
- [43] S. K. Mishra, F. Radu, S. Valencia, D. Schmitz, E. Schierle, H. A. Dürr, and W. Eberhardt, *Phys. Rev. B* **81**, 212404 (2010).
- [44] J. T. Kohlhepp and W. J. M. de Jonge, *J. Appl. Phys.* **95**, 6840 (2004).
- [45] V. K. Valev, A. Kirilyuk, F. Dalla Longa, J. T. Kohlhepp, B. Koopmans, and Th. Rasing, *Phys. Rev. B* **75**, 012401 (2007).
- [46] The distribution of I_A curves could be broader than expected because of the nonuniform x-ray profile.
- [47] T. Ambrose and C. L. Chien, *Phys. Rev. Lett.* **76**, 1743 (1996).
- [48] S. Fox and H. J. F. Jansen, *Phys. Rev. B* **60**, 4397 (1999).
- [49] A slight shift of hysteresis loops towards the negative field direction ($3 \sim 4$ Oe) may be caused by a not-perfect calibration between the magnetic field and applied current in the measurement system.
- [50] I. Di Marco, J. Minár, S. Chadov, M. I. Katsnelson, H. Ebert, and A. I. Lichtenstein, *Phys. Rev. B* **79**, 115111 (2009).
- [51] I. Di Marco, J. Minár, J. Braun, M. I. Katsnelson, A. Grechnev, H. Ebert, A. I. Lichtenstein, and O. Eriksson, *Eur. Phys. J. B* **72**, 473 (2009).